

Possible inversion symmetry breaking in the $S = 1/2$ pyrochlore Heisenberg magnet

Imre Hagymási,^{1,2,*} Robin Schäfer,^{3,†} Roderich Moessner,^{1,‡} and David J. Luitz^{1,§}

¹Max Planck Institute for the Physics of Complex Systems, Noethnitzer Str. 38, 01187 Dresden, Germany

²Strongly Correlated Systems "Lendület" Research Group, Institute for Solid State Physics and Optics, Wigner Research Centre for Physics, Budapest H-1525 P.O. Box 49, Hungary

³Max Planck Institute for the Physics of Complex Systems, Noethnitzer Strasse 38, 01187 Dresden, Germany

(Dated: March 22, 2021)

We address the ground-state properties of the long-standing and much-studied three-dimensional quantum spin liquid candidate, the $S = \frac{1}{2}$ pyrochlore Heisenberg antiferromagnet. By using $SU(2)$ DMRG, we are able to access cluster sizes of up to 128 spins. Our most striking finding is a robust spontaneous inversion symmetry breaking, reflected in an energy density difference between the two sublattices of tetrahedra, familiar as a starting point of earlier perturbative treatments. We also determine the ground-state energy, $E_0/N_{\text{sites}} = -0.490(6)J$, by combining extrapolations of DMRG with those of a numerical linked cluster expansion. These findings suggest a scenario in which a finite-temperature spin liquid regime gives way to a symmetry-broken state at low temperatures.

Introduction.— Frustrated magnets, on account of exhibiting many competing low energy states, are a fertile ground for exotic physics. A celebrated example is the pyrochlore Heisenberg antiferromagnet, which resides on a lattice of corner sharing tetrahedra, depicted in the inset of Fig. 1. The classical Heisenberg model on this lattice has a highly degenerate ground state [1], forming a classical spin liquid [2] with an emergent gauge field [3].

In contrast, the ground state of the quantum pyrochlore antiferromagnet remains enigmatic. While recent experimental evidence in the approximately isotropic $S = 1$ compound $\text{NaCaNi}_2\text{F}_7$ shows a liquid like state down to low temperature [4], the $S = 1/2$ case is still open both in theory and experiment.

Theory work on this prominent quantum spin liquid candidate over the years has been formidable. Absent a systematically controlled method, various approaches have somewhat inevitably led to an array of possible scenarios. One strand of work has built on a perturbative approach, in which half the couplings (those on one tetrahedral sublattice) are switched on perturbatively. This has led to suggestions of a ground state which breaks translational and rotational symmetries [5–7], a valence bond crystal [8] or a spin liquid state [9]. On top of this, the contractor renormalization method [10] finds antiferromagnetic ordering in a space of supertetrahedral pseudospins, pointing to an even larger real-space unit cell. To render the problem more tractable, all these theories involve the derivation of an effective Hamiltonian, which is *per se* not exactly solvable and hence solved by some type of approximation, ranging from mean field theory to classical Monte Carlo numerics. On a different axis in theory space, parton-based theories yield an ordered state with a chiral order parameter [15] or a monopole

flux state [17], while the pseudofermion functional renormalization group suggests a spin liquid ground state [18].

In view of this relatively wide range of ground-state candidates, a controlled and unbiased treatment of the model is clearly desirable, if only to narrow the possible location of the goalposts somewhat. Unfortunately, most numerical approaches quickly reach their limits for frustrated magnets in $d = 3$. While exact diagonalization is currently limited to ~ 48 sites [19], possible alternatives are series expansions such as the numerical linked cluster expansion (NLCE) [20–36] or high temperature expansions [37, 38], which can be pushed down to low temperatures [36], although they do not provide access to the ground state itself and are particularly challenged by many competing low energy states.

To access the ground-state wave function directly, the DMRG method — originally devised in one dimension [39–43] has been pushed to two dimensions, in particular for the two-dimensional cousin of pyrochlore, the kagome antiferromagnet [44–48].

Here, we take DMRG one step further, by applying it to the pyrochlore lattice in $d = 3$, and present a study of periodic clusters with $N_{\text{sites}} = 32, 48, 64, 108, 128$. This demonstrates that DMRG can treat clusters with up to 128 sites reliably, significantly larger than previous exact diagonalization results of 36 sites [49]. Exploiting the $SU(2)$ symmetry of the model [50–53], we keep up to 20000 $SU(2)$ states, (typically equivalent to $\gtrsim 80000$ $U(1)$ states). We calculate the ground-state energy, the spin structure factor and low-energy excitations for these clusters, yielding an estimate for the ground-state energy per site in the thermodynamic limit of $E_0/N_{\text{sites}} = -0.490(6)$. The study of finite size clusters is complemented by a high order NLCE calculation, which *excludes* any scenario where $E_0/N_{\text{sites}} > -0.471$.

Our main finding is that the ground state of the larger (64-, 108- and 128-site) clusters we consider exhibits a breathing instability, rendering up and down tetrahedra (cf. inset of Fig. 1) inequivalent: one tetrahedral sublattice exhibits a lower energy than the other. Amusingly,

* hagymasi@pks.mpg.de

† schaefer@pks.mpg.de

‡ moessner@pks.mpg.de

§ dluitz@pks.mpg.de

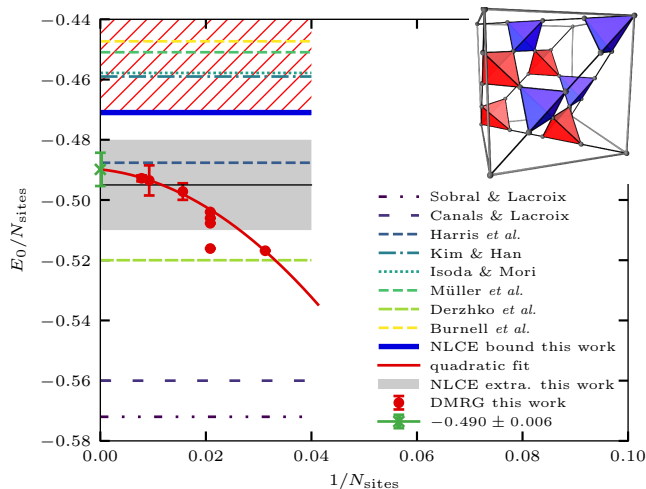


FIG. 1. Ground-state energies from various approaches. The horizontal lines denote the predictions for the ground-state energy per site ($J = 1$) in the thermodynamic limit: Sobral and Lacroix -0.572 [11], Canals and Lacroix -0.56 [12], Derzhko *et al.* -0.52 [13], Harris *et al.* -0.487 [5 and 14], Kim and Han -0.459 , [15], Isoda and Mori -0.4578 [8], Müller *et al.* -0.4509 [16], Burnell *et al.* -0.4473 [17]. The solid red points are our DMRG results for periodic clusters, extrapolated to infinite bond dimension using a quadratic polynomial. The thick blue line represents a robust upper bound for the ground-state energy, obtained from converged NLCE results at finite temperature, thus excluding the red hashed area. The solid black line shows the extrapolated value of the converged NLCE results to zero temperature (*cf.* Appendix D), and the gray shaded area indicates the confidence interval of this extrapolation. The inset shows the cubic unit cell of the pyrochlore lattice, highlighting the two tetrahedral sublattices in red and blue.

our estimate for the ground state energy is compatible with that of the original perturbation theory with a simple mean field solution of the resulting effective Hamiltonian, where the inversion symmetry was maximally broken at the very outset of the calculation [5].

Model and methods.— We consider the pyrochlore antiferromagnetic Heisenberg model with $S = 1/2$:

$$H = J \sum_{\langle i,j \rangle} \vec{S}_i \cdot \vec{S}_j, \quad (1)$$

where the spins sit on the sites i, j of the 3D pyrochlore lattice and $\langle i, j \rangle$ denotes nearest neighbors. The lattice is a face centered cubic lattice with lattice vectors $\vec{a}_1 = \frac{1}{2}(1, 1, 0)^T$, $\vec{a}_2 = \frac{1}{2}(1, 0, 1)^T$, $\vec{a}_3 = \frac{1}{2}(0, 1, 1)^T$ and a tetrahedral basis given by $\vec{b}_0 = \vec{0}$, $\vec{b}_1 = \frac{1}{2}\vec{a}_1$, $\vec{b}_2 = \frac{1}{2}\vec{a}_2$, $\vec{b}_3 = \frac{1}{2}\vec{a}_3$, such that each lattice point can be expressed by $\vec{R}_{\alpha, n_1, n_2, n_3} = n_1\vec{a}_1 + n_2\vec{a}_2 + n_3\vec{a}_3 + \vec{b}_\alpha$, with integer n_1, n_2, n_3 and $\alpha \in \{0, 1, 2, 3\}$. The model is obviously $SU(2)$ symmetric. Our DMRG calculations are performed on finite size ($N = 32, 48, 64, 108, 128$) clusters with periodic boundary conditions (*cf.* Tab. IV of Appendix).

We apply the one- and two-site variants of $SU(2)$ DMRG to reach high bond dimensions necessary to obtain reliable results in our three-dimensional clusters. Since DMRG requires a one-dimensional topology, we impose a one-dimensional “snake” path on the three-dimensional lattice, which defines the variational manifold. We use fully periodic clusters to reduce boundary effects and confirm that using a snake path which minimizes the bandwidth of the connectivity matrix improves convergence [36, 54, 55].

For small bond dimensions ($\chi \lesssim 2000$) we use the two-site version of the DMRG, and switch to the one-site variant to optimize the wave function for larger χ . Since the truncation error is not well defined in the one-site variant case (due to the subspace expansion [52]), we use the reliable two-site variance estimation to extrapolate towards the error-free case [56], because calculation of the full variance would be impractical due to its cost.

It turns out that even the calculation of the two-site variance becomes too costly for clusters with more than ~ 100 sites and bond dimensions $\gtrsim 8000$. In certain cases, we revert to the usage of the two-site DMRG and extrapolate as a function of the truncation error (*cf.* 108-site cluster).

Ground-state energy.— Using DMRG, we calculate the variational ground-state energy of finite clusters with high accuracy. By systematically increasing the bond dimension χ , we enlarge the variational manifold in a controlled way, such that we can extrapolate, $\chi \rightarrow \infty$, to the exact limit using a linear extrapolation as a function of the two-site variance (*cf.* Fig. 2). We use an estimate of the systematic extrapolation error given by half the distance between the extrapolated value and the last DMRG point.

Fig. 1 shows the extrapolated energies per lattice site of all finite clusters we considered in comparison with the available predicted ground-state energies in the literature. Our results show a monotonic growth of the ground-state energy as the number of sites is increased.

The periodic clusters we consider have either the full cubic (32, 108) or an increased or reduced (48a, 48b, 48c, 48d, 64, 128) symmetry of the pyrochlore lattice and represent the bulk due to the absence of a surface. The energies per site of different clusters as a function of inverse cluster size admit a fit to a quadratic polynomial, which we use to obtain an extrapolation to the thermodynamic limit. In order to get an estimate of the extrapolation error, we use Gaussian resampling, using the systematic DMRG error-bars as standard deviation. This yields our best estimate for the ground-state energy of $E_0/N_{\text{sites}} = -0.490(6)$. In this fit we considered only the cluster 48d among the 48-site clusters, which appears to be consistent with the other clusters, while other 48-site clusters have lower ground state energies.

Our extrapolated ($\chi \rightarrow \infty$) cluster energies and gaps are summarized in Table I. While the singlet gaps in the most symmetric clusters (32, 48d) are very small, the triplet gaps are sizable and roughly an order of magnitude

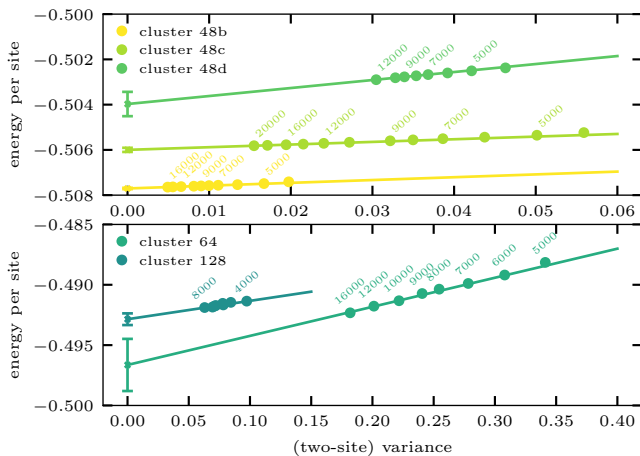


FIG. 2. Variational ground state energy estimates of the clusters 48b, 48c, 48d (top) and 64,128 (bottom) for different bond SU(2) bond dimensions χ (indicated by the labels) as a function of the two-site variance. Solid lines correspond to linear extrapolations to the error-free limit, corresponding to infinite bond dimension and zero variance. We estimate the systematic extrapolation error as the half distance between the last point and the extrapolated value.

larger. Since the 48d cluster does not obey all lattice symmetries, a reliable extrapolation is not possible, but our results are compatible with a scenario with a finite triplet gap, in which case all low energy excitations would be in the singlet sector as claimed in Refs. [6, 10].

Our finite temperature NLCE [20–36] provides a complementary perspective. We have carried out this expansion in entire tetrahedra up to eighth order (cf. [36] for details, as well as Appendix D), obtaining convergence for the energy per site in the thermodynamic limit as a function of temperature for temperatures $T \gtrsim 0.2$. Since the energy is a monotonic function of temperature, the converged part of $E(T)$ (cf. Fig. 8) provides an upper bound for the ground-state energy $E_{\text{nlce}} \approx -0.471J$, which is consistent with the DMRG data and extrapolation. One can furthermore polynomially extrapolate the finite temperature NLCE energies to zero temperature (assuming an analytic behavior at low temperatures), see Fig. 8, and obtain $-0.495(15)$, which agrees remarkably well with the DMRG extrapolation and lies within its error bar, serving as a further corroboration of the DMRG energy. In light of these results we can confidently exclude a ground-state energy per site larger than $-0.47J$.

Ground-state symmetry-breaking.— To investigate the properties of the ground state in more detail, we calculate the total spin, and hence total energy, of up and down tetrahedra separately. This reveals an inequivalence of up and down tetrahedra (cf. Fig. 6 in the Appendix), suggesting a breaking of the inversion symmetry of the lattice. In our DMRG calculations, the snake path does not fully respect the symmetry between up and down tetrahedra, so we need to verify that this symmetry breaking is intrinsic, and not due to a preference imposed by the

Cluster	GS energy	Singlet gap	Triplet gap
32	-0.5168	0.0318	0.6872
48a	-0.5161	0.2166(4)	0.6709(4)
48b	-0.5077	0.027(2)	0.554(2)
48c	-0.5060(1)	0.053(7)	0.42(2)
48d	-0.5040(5)	0.06(3)	0.36(3)
64	-0.4972(25)	—	—
108	-0.4935(50)	—	—
128	-0.4928(10)	—	—

TABLE I. Ground-state energies per site and gaps within the $S_{\text{tot}} = 0$ sector (singlet gap) as well as to the $S_{\text{tot}} = 1$ sector (triplet gap) if available.

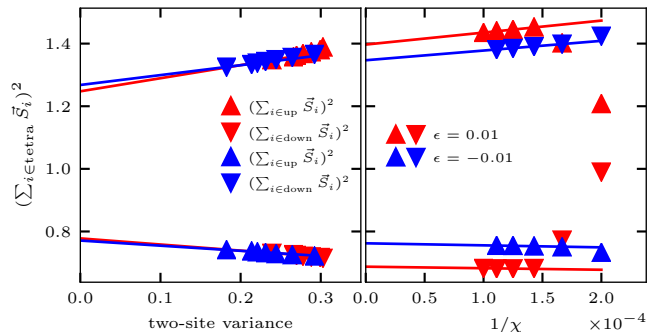


FIG. 3. Extrapolation of tetrahedron spins for an explicit breaking of lattice inversion symmetry, similarly to a “pinning” coupling, for the 64 (left) and 108 (right) site clusters. The whole Hamiltonian (1) is written as $H = (1-\epsilon)H_{\text{up}} + (1+\epsilon)H_{\text{down}}$, where the H_{up} and H_{down} parts contain the terms for the up and down tetrahedra, respectively.

snake path. We therefore introduce a small symmetry breaking ‘breathing’ perturbation, where we modify the couplings of up and down tetrahedra to be $J = 1 \pm \epsilon$, equivalent to the standard technique of including pinning fields.

Fig. 3 shows the results for the total spin of up and down tetrahedra for opposite signs of the breathing perturbation in the 64 (108) site clusters as a function of the two-site variance (inverse bond dimension), admitting a linear extrapolation towards $\chi \rightarrow \infty$. The results reveal a clear selection of states with opposite symmetry breaking, as required for spontaneous symmetry-breaking. The order parameters for the larger, 108-site, cluster are slightly different for the two opposite pinning fields (Fig. 3, right panel), but that difference is much smaller than the extrapolated order parameter which differs only little between the two clusters. It is of course always possible in principle that the symmetry breaking vanishes when yet larger clusters are considered. Given the scaling of the computational effort with system size, the study of much larger clusters with the present method is, however, out of reach. In Appendix A we provide further evidence that the two symmetry-breaking states

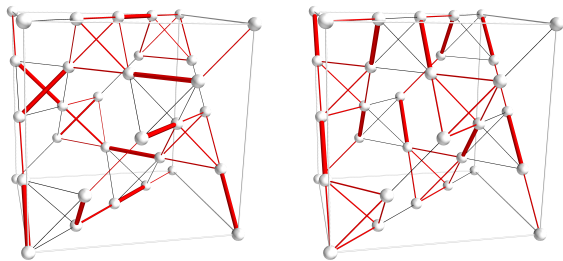


FIG. 4. Real space spin correlation C_{ij} in the ground state ($S_z = 0$) for $N = 64$ (left) and $N = 128$ (right) shown in the cubic unit cell. The thickness of the red bonds corresponds to magnitude of the correlation between neighboring sites. The black lines indicate bonds between sites with negligible correlations.

converge to the same energy after the pinning field is removed.

We next consider nearest neighbor spin correlations of the best (lowest-energy) wave functions $|\psi_0\rangle$ obtained in DMRG. For each pair of adjacent sites (i, j) , we calculate the correlation function $C_{ij} = \langle \psi_0 | \vec{S}_i \cdot \vec{S}_j | \psi_0 \rangle$. We plot the result for the clusters 64 and 128 in Fig. 4 (truncated to the cubic unit cell for ease of visualization), with the tube thickness proportional to the strength of the spin correlations.

The correlation pattern reveals that one sublattice (say, ‘up’) of tetrahedra contains more strongly correlated bonds than the other. These are found on opposite edges of ‘up’ tetrahedra. We note that the details of this pattern still depend strongly on the cluster geometry and we get opposite choices of correlated bonds in the two clusters, presumably due to different symmetry broken states picked by the different ‘snake’ paths in the two clusters. Moreover, the periodic boundary conditions impact the performance of the DMRG calculation. In particular, finite-sized clusters with periodic boundary conditions comprise winding loops which may be as short as, or even shorter, than the ‘physical’ loops in the bulk, whose minimal length is the circumference (6) of a hexagon. Resonances along both loop types will therefore compete. The minimal length of winding loops for $N = 108$ is 6 while it is 8 for $N = 128$. Indeed, we observe considerably better convergence for the latter, inducing a smaller error, see Fig. 1. The shortest periodic loop of each cluster is shown in Tab. IV.

Ground-state structure factor. — The static spin structure factor for different clusters, accessible in neutron scattering experiments, is obtained from the Fourier transform of the spin correlations (factor $4/3$ from normalization $1/(S(S+1))$ for spin $S = 1/2$):

$$S(\vec{Q}) = \frac{4}{3N} \sum_{ij} \langle \vec{S}_i \cdot \vec{S}_j \rangle_c \cos \left[\vec{Q} \cdot (\vec{R}_i - \vec{R}_j) \right], \quad (2)$$

where \vec{R}_i denote the real-space coordinates of sites and the index c denotes the connected part of the correlation

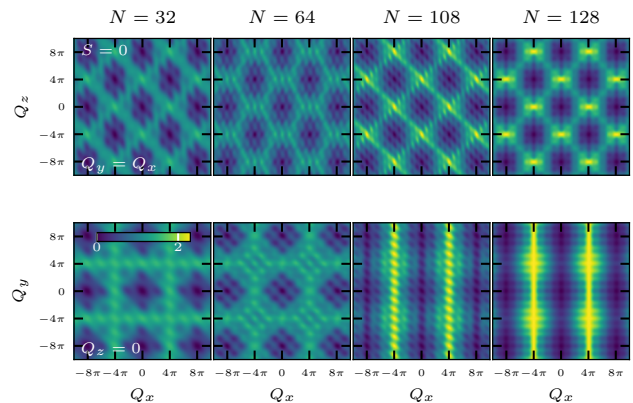


FIG. 5. Static spin structure factor for different clusters for two cuts ($Q_x = Q_y$ (top) and $Q_z = 0$ (bottom)) through momentum space. The corresponding maximal bond dimensions for the 32, 64, 108 and 128-site clusters are 20000, 16000, 16000 and 12000 respectively.

matrix. The results for two cuts ($Q_x = Q_y$ (top) and $Q_z = 0$ (bottom)) in the three-dimensional momentum space are shown in Fig. 5.

One can readily recognize the bow-tie patterns, the hallmark of pyrochlore magnets [3–5, 9, 16, 18, 36]. Note that the 32- and 108-site clusters have full cubic symmetry, while the 64-site cluster does not, hence the structure factors looks slightly different in that case. The results for the spin structure factor and the absence of sharp Bragg peaks confirm that there is no long range magnetic ordering. The observed pattern for the $Q_x = Q_y$ cuts is very close to what is found at finite temperature in the regime $T \lesssim 1$ [36], on the other hand the $Q_z = 0$ cuts exhibit a drastic change in the 108- and 128-site clusters reflecting the symmetry breaking. While the pinch points sharpen with increasing system size (and therefore momentum resolution), we are unable to extrapolate their width reliably to the thermodynamic limit to extract a correlation length. Note that for the largest clusters, apparent lines in the spin structure factor in the Q_x - Q_y plane become discernible, Fig. 4, raising the possibility of at least short-range spin correlations with spatial anisotropy. A more detailed search for such symmetry breaking is clearly warranted.

Concluding discussion. — Our DMRG study has found the ground state of the $SU(2)$ symmetric $S = \frac{1}{2}$ Heisenberg antiferromagnet to discard lattice inversion symmetry in favour of a ‘breathing’ pattern of strong (weak) sublattices of up (down) tetrahedra. We extrapolate the energy per lattice site to $-0.490(6)$. The possibility of such *spontaneous* symmetry breaking has been a central question for this class of magnets, as several studies have used an *explicit* such symmetry breaking as a starting point of various perturbative schemes [5, 6, 10, 57]. As the restoration of an explicitly broken symmetry in a perturbative scheme is generically not to be expected, a nonvanishing order parameter does not per se indicate

spontaneous symmetry breaking.

Our results are thus important in that they provide largely unbiased evidence for the existence of this spontaneous symmetry-breaking, subject only to finite-size effects which are much reduced in comparison to previous studies. This also indicates that one of the prime Heisenberg quantum spin liquid candidates in three dimensions in fact exhibits at least one form of symmetry breaking.

In closing, we note that our extrapolated ground-state energy lies close to the estimate obtained in the pioneering work by Harris *et al.* [5], in the abovementioned scheme of coupling the up tetrahedra perturbatively through the bonds of the down tetrahedra. These authors also found a long-range dimer ordering (cf. also [6]) compatible with the correlation pattern we observe in our calculations shown in Fig. 4. This first, simple and quite uncontrolled, approach to this difficult problem thus may turn out to have been already quite close

to what will eventually be established as the final answer.

ACKNOWLEDGMENTS

We thank Owen Benton, Ludovic Jaubert, Paul McClarty, Jeffrey Rau, Johannes Richter, Oleg Derzhko, Masafumi Udagawa and Karlo Penc for very helpful discussions. We acknowledge financial support from the Deutsche Forschungsgemeinschaft through SFB 1143 (Project-id 247310070) and cluster of excellence ct.qmat (EXC 2147, Project-id 390858490). I.H. was supported in part by the Hungarian National Research, Development and Innovation Office (NKFIH) through Grant No. K120569 and the Hungarian Quantum Technology National Excellence Program (Project No. 2017-1.2.1-NKP-2017-00001). Some of the data presented here was produced using the SYTEN toolkit, originally created by Claudius Hubig.[50, 51]

-
- [1] Jacques Villain, “Insulating spin glasses,” *Zeitschrift für Physik B Condensed Matter* **33**, 31–42 (1979).
- [2] R. Moessner and J. T. Chalker, “Properties of a classical spin liquid: The heisenberg pyrochlore antiferromagnet,” *Phys. Rev. Lett.* **80**, 2929–2932 (1998).
- [3] S. V. Isakov, K. Gregor, R. Moessner, and S. L. Sondhi, “Dipolar Spin Correlations in Classical Pyrochlore Magnets,” *Phys. Rev. Lett.* **93**, 167204 (2004), [arXiv:cond-mat/0407004 \[cond-mat.dis-nn\]](#).
- [4] K. W. Plumb, Hitesh J. Changlani, A. Scheie, Shu Zhang, J. W. Krizan, J. A. Rodriguez-Rivera, Yiming Qiu, B. Winn, R. J. Cava, and C. L. Broholm, “Continuum of quantum fluctuations in a three-dimensional $S = 1$ Heisenberg magnet,” *Nature Physics* **15**, 54–59 (2019).
- [5] A. B. Harris, A. J. Berlinsky, and C. Bruder, “Ordering by quantum fluctuations in a strongly frustrated Heisenberg antiferromagnet,” *Journal of Applied Physics* **69**, 5200 (1991).
- [6] Hirokazu Tsunetsugu, “Spin-singlet order in a pyrochlore antiferromagnet,” *Phys. Rev. B* **65**, 024415 (2001).
- [7] Hirokazu Tsunetsugu, “Antiferromagnetic quantum spins on the pyrochlore lattice,” *Journal of the Physical Society of Japan* **70**, 640–643 (2001).
- [8] Makoto Isoda and Shigeyoshi Mori, “Valence-Bond Crystal and Anisotropic Excitation Spectrum on 3-Dimensionally Frustrated Pyrochlore,” *Journal of the Physical Society of Japan* **67**, 4022–4025 (1998).
- [9] B. Canals and C. Lacroix, “Pyrochlore antiferromagnet: A three-dimensional quantum spin liquid,” *Phys. Rev. Lett.* **80**, 2933–2936 (1998).
- [10] Erez Berg, Ehud Altman, and Assa Auerbach, “Singlet excitations in pyrochlore: A study of quantum frustration,” *Physical Review Letters* **90** (2003), [10.1103/physrevlett.90.147204](#).
- [11] R.R. Sobral and C. Lacroix, “Order by disorder in the pyrochlore antiferromagnets,” *Solid State Communications* **103**, 407 – 409 (1997).
- [12] Benjamin Canals and Claudine Lacroix, “Quantum spin liquid: The heisenberg antiferromagnet on the three-dimensional pyrochlore lattice,” *Phys. Rev. B* **61**, 1149–1159 (2000).
- [13] Oleg Derzhko, Taras Hutak, Taras Krokhmal'skii, Jürgen Schnack, and Johannes Richter, “Adapting planck’s route to investigate the thermodynamics of the spin-half pyrochlore heisenberg antiferromagnet,” *Phys. Rev. B* **101**, 174426 (2020).
- [14] Akihisa Koga and Norio Kawakami, “Frustrated heisenberg antiferromagnet on the pyrochlore lattice,” *Phys. Rev. B* **63**, 144432 (2001).
- [15] Jung Hoon Kim and Jung Hoon Han, “Chiral spin states in the pyrochlore heisenberg magnet: Fermionic mean-field theory and variational monte carlo calculations,” *Phys. Rev. B* **78**, 180410 (2008).
- [16] Patrick Müller, Andre Lohmann, Johannes Richter, and Oleg Derzhko, “Thermodynamics of the pyrochlore-lattice quantum Heisenberg antiferromagnet,” *Phys. Rev. B* **100**, 024424 (2019).
- [17] F. J. Burnell, Shoibal Chakravarty, and S. L. Sondhi, “Monopole flux state on the pyrochlore lattice,” *Physical Review B* **79**, 144432 (2009).
- [18] Yasir Iqbal, Tobias Müller, Pratyay Ghosh, Michel J. P. Gingras, Harald O. Jeschke, Stephan Rachel, Johannes Reuther, and Ronny Thomale, “Quantum and Classical Phases of the Pyrochlore Heisenberg Model with Competing Interactions,” *Phys. Rev. X* **9**, 011005 (2019).
- [19] Andreas M. Läuchli, Julien Sudan, and Roderich Moessner, “ $s = \frac{1}{2}$ kagome heisenberg antiferromagnet revisited,” *Phys. Rev. B* **100**, 155142 (2019).
- [20] Marcos Rigol, Tyler Bryant, and Rajiv R. P. Singh, “Numerical linked-cluster approach to quantum lattice models,” *Phys. Rev. Lett.* **97**, 187202 (2006).
- [21] Marcos Rigol, Tyler Bryant, and Rajiv R. P. Singh, “Numerical linked-cluster algorithms. ii. $t-j$ models on the square lattice,” *Phys. Rev. E* **75**, 061119 (2007).
- [22] Marcos Rigol, Tyler Bryant, and Rajiv R. P. Singh, “Numerical linked-cluster algorithms. i. spin systems on square, triangular, and kagomé lattices,” *Phys. Rev. E* **75**, 061118 (2007).

- [23] Ehsan Khatami and Marcos Rigol, “Thermodynamics of the antiferromagnetic heisenberg model on the checkerboard lattice,” *Phys. Rev. B* **83**, 134431 (2011).
- [24] Ehsan Khatami, Joel S. Helton, and Marcos Rigol, “Numerical study of the thermodynamics of clinoatacamite,” *Phys. Rev. B* **85**, 064401 (2012).
- [25] Ehsan Khatami, Rajiv R. P. Singh, and Marcos Rigol, “Thermodynamics and phase transitions for the heisenberg model on the pinwheel distorted kagome lattice,” *Phys. Rev. B* **84**, 224411 (2011).
- [26] Ehsan Khatami and Marcos Rigol, “Thermodynamics of strongly interacting fermions in two-dimensional optical lattices,” *Phys. Rev. A* **84**, 053611 (2011).
- [27] Ehsan Khatami and Marcos Rigol, “Effect of particle statistics in strongly correlated two-dimensional hubbard models,” *Phys. Rev. A* **86**, 023633 (2012).
- [28] R. Applegate, N. R. Hayre, R. R. P. Singh, T. Lin, A. G. R. Day, and M. J. P. Gingras, “Vindication of $\text{Yb}_2\text{T}_2\text{O}_7$ as a model exchange quantum spin ice,” *Phys. Rev. Lett.* **109**, 097205 (2012).
- [29] R. R. P. Singh and J. Oitmaa, “Corrections to pauling residual entropy and single tetrahedron based approximations for the pyrochlore lattice using antiferromagnet,” *Phys. Rev. B* **85**, 144414 (2012).
- [30] Baoming Tang, Ehsan Khatami, and Marcos Rigol, “A short introduction to numerical linked-cluster expansions,” *Computer Physics Communications* **184**, 557 – 564 (2013).
- [31] N. R. Hayre, K. A. Ross, R. Applegate, T. Lin, R. R. P. Singh, B. D. Gaulin, and M. J. P. Gingras, “Thermodynamic properties of $\text{Yb}_2\text{T}_2\text{O}_7$ pyrochlore as a function of temperature and magnetic field: Validation of a quantum spin ice exchange hamiltonian,” *Phys. Rev. B* **87**, 184423 (2013).
- [32] L. D. C. Jaubert, Owen Benton, Jeffrey G. Rau, J. Oitmaa, R. R. P. Singh, Nic Shannon, and Michel J. P. Gingras, “Are multiphase competition and order by disorder the keys to understanding $\text{yb}_2\text{t}_2\text{o}_7$?” *Phys. Rev. Lett.* **115**, 267208 (2015).
- [33] Owen Benton, L. D. C. Jaubert, Rajiv R. P. Singh, Jaan Oitmaa, and Nic Shannon, “Quantum spin ice with frustrated transverse exchange: From a π -flux phase to a nematic quantum spin liquid,” *Phys. Rev. Lett.* **121**, 067201 (2018).
- [34] Owen Benton, “Instabilities of a $u(1)$ quantum spin liquid in disordered non-kramers pyrochlores,” *Phys. Rev. Lett.* **121**, 037203 (2018).
- [35] Tom Pardini, Anirudha Menon, Stefan P. Hau-Riege, and Rajiv R. P. Singh, “Local entanglement and confinement transitions in the random transverse-field ising model on the pyrochlore lattice,” *Phys. Rev. B* **100**, 144437 (2019).
- [36] Robin Schäfer, Imre Hagymási, Roderich Moessner, and David J. Luitz, “Pyrochlore $s = \frac{1}{2}$ Heisenberg antiferromagnet at finite temperature,” *Physical Review B* **102**, 054408 (2020), publisher: American Physical Society.
- [37] Andre Lohmann, Heinz-Jürgen Schmidt, and Johannes Richter, “Tenth-order high-temperature expansion for the susceptibility and the specific heat of spin- $\frac{1}{2}$ Heisenberg models with arbitrary exchange patterns: Application to pyrochlore and kagome magnets,” *Physical Review B* **89**, 014415 (2014).
- [38] Jonas Richter and Robin Steinigeweg, “Combining dynamical quantum typicality and numerical linked cluster expansions,” *Phys. Rev. B* **99**, 094419 (2019).
- [39] Steven R. White, “Density matrix formulation for quantum renormalization groups,” *Phys. Rev. Lett.* **69**, 2863–2866 (1992).
- [40] Steven R. White, “Density-matrix algorithms for quantum renormalization groups,” *Phys. Rev. B* **48**, 10345–10356 (1993).
- [41] Reinhard M. Noack, Salvatore R. Manmana, Adolfo Avella, and Ferdinando Mancini, “Diagonalization and numerical renormalization-group-based methods for interacting quantum systems,” *AIP Conference Proceedings* **789**, 93–163 (2005), <https://aip.scitation.org/doi/pdf/10.1063/1.2080349>.
- [42] Ulrich Schollwöck, “The density-matrix renormalization group in the age of matrix product states,” *Annals of Physics* **326**, 96 – 192 (2011), january 2011 Special Issue.
- [43] Karen A. Hallberg, “New trends in density matrix renormalization,” *Advances in Physics* **55**, 477–526 (2006), <https://doi.org/10.1080/00018730600766432>.
- [44] Stefan Depenbrock, Ian P. McCulloch, and Ulrich Schollwöck, “Nature of the spin-liquid ground state of the $s = 1/2$ heisenberg model on the kagome lattice,” *Phys. Rev. Lett.* **109**, 067201 (2012).
- [45] Hong-Chen Jiang, Zhenghan Wang, and Leon Balents, “Identifying topological order by entanglement entropy,” *Nature Physics* **8**, 902–905 (2012).
- [46] Simeng Yan, David A. Huse, and Steven R. White, “Spin-liquid ground state of the $s = 1/2$ kagome heisenberg antiferromagnet,” *Science* **332**, 1173–1176 (2011).
- [47] Yin-Chen He, Michael P. Zaletel, Masaki Oshikawa, and Frank Pollmann, “Signatures of dirac cones in a dmrg study of the kagome heisenberg model,” *Phys. Rev. X* **7**, 031020 (2017).
- [48] H. C. Jiang, Z. Y. Weng, and D. N. Sheng, “Density matrix renormalization group numerical study of the kagome antiferromagnet,” *Phys. Rev. Lett.* **101**, 117203 (2008).
- [49] V. Ravi Chandra and Jyotisman Sahoo, “Spin-1/2 Heisenberg antiferromagnet on the pyrochlore lattice: An exact diagonalization study,” *Physical Review B* **97**, 144407 (2018).
- [50] Claudius Hubig, Felix Lachenmaier, Nils-Oliver Linden, Teresa Reinhard, Leo Stenzel, Andreas Swoboda, and Martin Grundner, “The SYTEN toolkit,” .
- [51] Claudius Hubig, *Symmetry-Protected Tensor Networks*, Ph.D. thesis, LMU München (2017).
- [52] C. Hubig, I. P. McCulloch, U. Schollwöck, and F. A. Wolf, “Strictly single-site dmrg algorithm with subspace expansion,” *Phys. Rev. B* **91**, 155115 (2015).
- [53] Ian P McCulloch, “From density-matrix renormalization group to matrix product states,” *Journal of Statistical Mechanics: Theory and Experiment* **2007**, P10014–P10014 (2007).
- [54] U. Schollwöck, “The density-matrix renormalization group,” *Rev. Mod. Phys.* **77**, 259–315 (2005).
- [55] J. Ummethum, J. Schnack, and A. M. Läuchli, “Large-scale numerical investigations of the antiferromagnetic heisenberg icosidodecahedron,” *Journal of Magnetism and Magnetic Materials* **327**, 103 – 109 (2013).
- [56] C. Hubig, J. Haegeman, and U. Schollwöck, “Error estimates for extrapolations with matrix-product states,” *Phys. Rev. B* **97**, 045125 (2018).
- [57] R. Moessner, S. L. Sondhi, and M. O. Goerbig, “Quantum dimer models and effective hamiltonians on the pyrochlore lattice,” *Physical Review B* **73** (2006),

10.1103/physrevb.73.094430.

Appendix A: Inversion-symmetry breaking

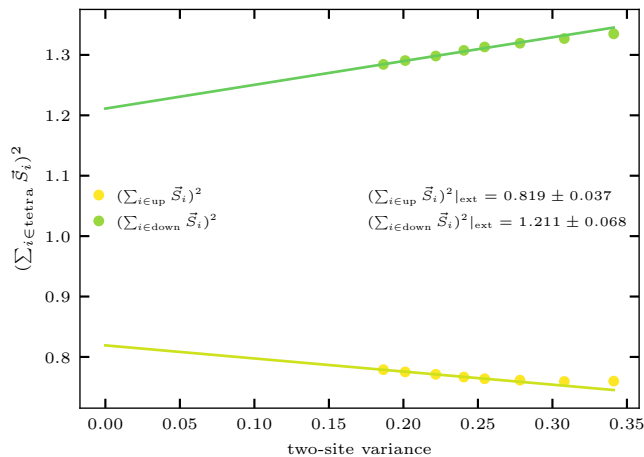


FIG. 6. The extrapolation of the total spin squared as a function of the two-site variance for the 64-site cluster.

The real space dimer correlation pattern shown in Fig. 4 suggests that the lattice inversion symmetry is broken in the ground state. In order to scrutinize this finding, we analyze the square of the total spin (morally the tetrahedron energy) of up and down tetrahedra in the lattice separately. Fig. 6 shows the extrapolation to the exact limit for the 64 site cluster. The extrapolation clearly suggests an imbalance between up and down tetrahedra, and confirms the finding from the real space dimer correlations. This is further corroborated by a high susceptibility towards inversion symmetry breaking perturbations, as discussed in the main text. In order to determine whether the applied pinning, $\epsilon = 0.01$ is sufficiently small, we apply the following DMRG procedure. For a given ordering of the sites, the symmetry-breaking state involving the least entanglement, is preferred by DMRG. Our strategy is as follows: we perform DMRG calculations up to a certain bond dimension (with the pinning applied), until the states are stabilized. Then we switch off the pinning ($\epsilon \rightarrow 0$) and perform further sweeping and increase the bond dimension. If the symmetry breaking is intrinsic, both of these energies should agree with each other, and with the one without pinning. We carried out this test for the 64-site cluster and find that if the pinning is removed too early (for example with 3000 states) DMRG converges back to the state preferred by the snake. However, the state becomes stable at bond dimension 5000 and remains so for the further increase of the bond dimension and sweeping. Obviously, this problem is not present if the pinning as well as the snake prefer the same state. Considering the energies, a smooth linear extrapolation is possible (Fig. 7) and each of them results in the same energy lying well within the error bars.

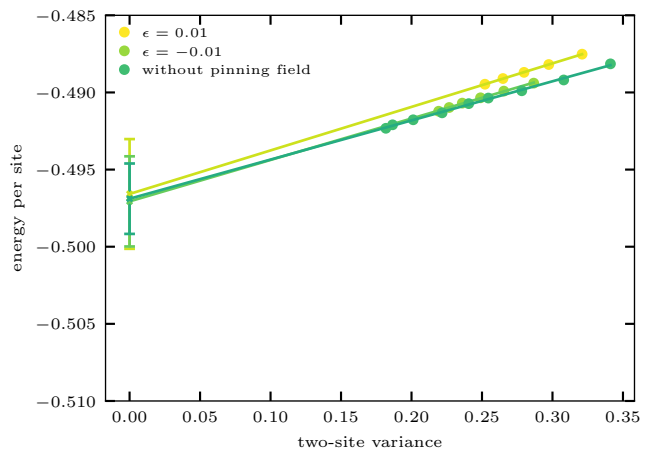


FIG. 7. The extrapolation of the energies after the pinning field is switched off together with the one without the pinning field for the 64-site cluster.

Appendix B: Other lattice symmetries

We further investigated various symmetries with respect to our ground state correlations shown in Fig. 4 for the clusters with $N = 64$ and $N = 128$. As mentioned in the main text, resonant loops across periodic boundary conditions compete with the loops in the bulk. The cluster with $N = 108$ exhibits loops across the boundary of length 6 which compete with bulk hexagonal loops. Therefore, the correlation pattern of the $N = 108$ appears defective in some regions if compared to the pattern obtained for $N = 128$ with loops across the boundary of length 8. For the $N = 64$ cluster, also boundary loops of length 6 appear. The last column of table IV lists the length of the shortest boundary loops in all clusters we investigated.

To analyze the symmetries of the observed correlation pattern, we start by coarse graining it. There are three different types of bonds. First, we find six uniformly weakly coupled bonds (A) on one type of the tetrahedra. Second, the inverted tetrahedra exhibit two types of bonds, two strong dimers (B) and four vanishing bonds (C). The average correlation strengths of each bond type are listed in Table II for $N = 64$ and $N = 128$. The simplified nearest neighbor correlation pattern can then be viewed as a graph with edges labeled by A , B , or C .

Each lattice symmetry is a permutation $\pi \in S_N$ of nodes in this graph. The type X of an edge (i, j) is preserved under the symmetry transformation if $(\pi(i), \pi(j))$ is of the same type X . Applying all lattice symmetries to the labeled graphs for our largest clusters, $N = 64$ and $N = 128$, we can count how many edges preserve their type under the symmetry and list the ratio the ratio c/t of conserved edges c over the number of total edges $t = 3N$ in Table III for all lattice symmetries.

From this systematic symmetry analysis, it is clear that the correlation pattern is fully symmetric for $N = 128$

	<i>A</i>	<i>B</i>	<i>C</i>
64	-0.14339314	-0.53707564	-0.00869636
128	-0.14484361	-0.53011351	-0.00968693

TABLE II. Averaged correlation strength of three types of *A*, *B* and *C* observed in the real space correlations in Fig. 4 starting from the simplified picture. 12 of 192 bonds for the $N = 64$ and none of the 384 bonds for $N = 128$ violate the simplified picture.

	64	128
$3_{(x,x,x)}^+$	136/192	256/384
$3_{(x,x,x)}^-$	136/192	256/384
$2_{(0,-y,y)}$	4/192	0/384
$2_{(-x,0,x)}$	12/192	0/384
$2_{(x,-x,0)}$	4/192	0/384
$I_{(0,0,0)}$	10/192	0/384
$3_{(x,x,x)}^+ I_{(0,0,0)}$	10/192	0/384
$3_{(x,x,x)}^- I_{(0,0,0)}$	10/192	0/384
$m_{(x,y,y)}$	152/192	384/384
$m_{(x,y,x)}$	144/192	256/384
$m_{(x,x,y)}$	136/192	256/384
$T_{(1,0,0)}$	136/192	384/384
$T_{(0,1,0)}$	136/192	384/384
$T_{(0,0,1)}$	132/192	384/384
$T_{(1,1,0)}$	132/192	384/384
$T_{(1,0,1)}$	136/192	384/384
$T_{(0,1,1)}$	136/192	384/384

TABLE III. Ratio of the number of conserved edges over the number of total edges $3N$ for different symmetry operations. $k_{(x,y,z)}^\pm$ describes a rotation by $\pm 2\pi/k$ around the axis (x, y, z) , $I_{(0,0,0)}$ is the inversion around the center and $m_{(x,y,z)}$ is a reflection. The second part of the table considers translations of the form $T_{(a,b,c)}$ which describes a shift by $a\vec{a}_1 + b\vec{a}_2 + c\vec{a}_3$.

under all fcc translations $T_{(a,b,c)}$, which means that each tetrahedron shows the same orientation of strong dimers. This leads to quasi decoupled planes of weakly coupled tetrahedra connected by strong dimers in this cluster.

On the other hand, all symmetry operations matching one type of tetrahedra to another (in particular inversion) are robustly broken, since in both $N = 64$ and $N = 128$ clusters the number of type preserved bonds is essentially zero.

The $N = 64$ cluster confirms this picture. Due to the competition of length 6 boundary loops with bulk hexagonal looks, the correlation pattern is slightly defective if compared to $N = 128$, which leads to slightly imperfect preservation of the pattern under symmetry operations. The orientation of the strong bonds *B* seem to be arbitrary.

Appendix C: Finite-size clusters

We use the clusters 32, 48a, 48b, 48c, 48d, 64, 108, and 128 in our simulations, which are described by the cluster vectors $\vec{c}_1, \vec{c}_2, \vec{c}_3$. The performance of the DMRG calculation is affected by loops winding across the periodic boundaries. The key element is the length of these winding loops compared to resonant loops within the bulk (predominantly hexagons). Therefore, Tab. IV lists the length of the shortest loop connected via a periodic bond for each cluster.

cluster	\vec{c}_1	\vec{c}_2	\vec{c}_3	length
32	$2\vec{a}_1$	$2\vec{a}_2$	$2\vec{a}_3$	4
48a	$(\frac{3}{2}, \frac{1}{2}, 0)^T$	$(0, 1, 1)^T$	$(0, 1, -1)^T$	4
48b	$(\frac{3}{2}, \frac{1}{2}, 0)^T$	$(0, \frac{1}{2}, \frac{3}{2})^T$	$(0, 1, -1)^T$	4
48c	$(\frac{3}{2}, 1, \frac{1}{2})^T$	$(0, 1, -1)^T$	$(1, -1, 0)^T$	4
48d	$(1, 1, 1)^T$	$(1, 0, -1)^T$	$(1, -1, 0)^T$	4
64	$(1, 1, 1)^T$	$(1, 1, -1)^T$	$(-1, 1, 1)^T$	6
108	$3\vec{a}_1$	$3\vec{a}_2$	$3\vec{a}_3$	6
128	$(2, 0, 0)^T$	$(0, 2, 0)^T$	$(0, 0, 2)^T$	8

TABLE IV. Cluster vectors $\vec{c}_1, \vec{c}_2, \vec{c}_3$ of the 8 clusters used in this work and the length of the shortest periodic loop. The clusters of size 32 and 108 respect all lattice symmetries.

Appendix D: Numerical linked cluster expansion

We apply a systematic high temperature series expansion to obtain an upper bound for the ground state energy of pyrochlore lattice in the thermodynamic limit. The numerical linked cluster expansion (NLCE) determines any extensive property P (such as the energy) in the high temperature regime. It has been successfully applied to various geometries including frustrated systems like the kagome or pyrochlore lattice [20–35].

A detailed description of the approach used here can be found in our previous work [36]. It has been shown that an expansion based on *tetrahedra* provides the most efficient approach, yielding reliably converged energy results down to temperatures $T \gtrsim 0.2$. Here, we include all clusters with full exact diagonalization consisting of up to 8 tetrahedra (i.e. up to 25 spins $\frac{1}{2}$). These clusters include crucial loops of 6 and 8 spins.

Since the energy decreases monotonously with temperature, we are able use the converged part as an upper bound for the ground state energy ($E_{\text{nlce}} \approx -0.471J$) in the thermodynamic limit. Assuming an analytic behavior we used the converged part in the finite temperature regime to predict the zero temperature ground state energy. Hence, we extrapolated the function using a quadratic polynomial:

$$E(T) = a + bT + cT^2. \quad (\text{D1})$$

The range of the best fit is between the convergence limit at $T \approx 0.25$ and $T = 0.5$, and we varied the range limits randomly to estimate the systematic error of the fit, yielding $E_{\text{extra}} \approx -0.495(15)$.

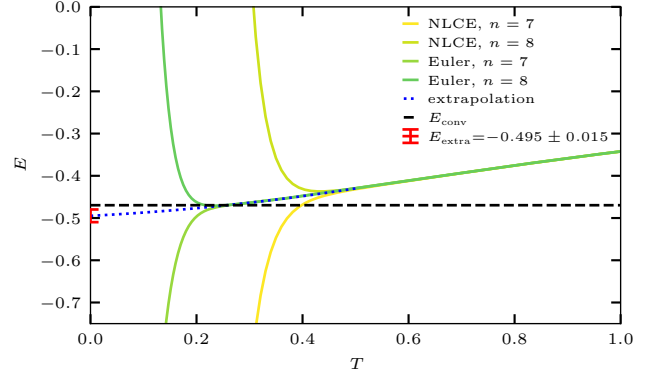


FIG. 8. Energy per site with NLCE expansion up 8th order in combination with the euler series acceleration with $k = 3$ [36]. The energy in the thermodynamic limit is converged down to $T \approx 0.25$ in units of J with a value of $E_{\text{nlce}} \approx -0.471J$. This can be used as an upper bound for the ground state energy. Additionally, we extrapolated the converged part with a simple quadratic *ansatz* and received an extrapolated ground state energy of $-0.495J$.